INTERNATIONAL JOURNAL OF AUTOMOTIVE AND MECHANICAL ENGINEERING
ISSN: 2229-8649 e-ISSN: 2180-1606
VOL. 21, ISSUE 4, 2024, 11757 – 11769
DOI: https://doi.org/10.15282/ijame.21.4.2024.3.0906

RESEARCH ARTICLE

Performance Characteristics of a Compact Core Annular-Radial Magnetorheological Damper for Vehicle Suspension Systems

A.Z. Zainordin[1]*, Z. Mohamed[2]*

[1]Department of Mechanical Engineering, Politeknik Sultan Haji Ahmad Shah, 25350 Kuantan, Pahang, Malaysia
[2]Faculty of Mechanical and Automotive Engineering Technology, Universiti Malaysia Pahang Al-Sultan Abdullah, 26600 Pahang, Malaysia

ABSTRACT – The magnetorheological (MR) damper is a by-wire system capable of providing variable damping stiffness by responding to an apparent magnetic field. In response to the magnetic field application, the magnetorheological fluid (MR fluid) exhibited altered behavior within the damper. Typically, a damper's internal and external valves operate in flow mode, where the flow is regulated by controlling the magnetic field. This study aims to investigate the performance characteristics of a small core annular and radial magnetorheological valve (SCARMV) designed for applications in vehicle suspension systems. The proposed design of the simplified MR valve is based on a meandering-type valve composed of multiple valve cores that have been simplified to a single core. Dynamic testing was performed on the proposed valve, which features a single rod tube damper, to investigate the damping force characteristics by varying currents and frequencies. The characteristics of the measured damping force were compared to the calculated damping force based on the pressure drop calculation and the FEMM simulation of magnetic flux. By increasing the stroke length of the valve travel is set to 10 mm at a current input of 0 A to 1.0 A, the maximum output of the MR valve damping force was approximately 1.57 kN. In addition, a mathematical model of SCARMV is presented and compared to the experimental data. Therefore, based on the experimental results, it was concluded that the usability of a compact core MR valve is reliable. However, more in-depth studies are required before these dampers can be applied to vehicle suspension systems.

ARTICLE HISTORY

Received	:	09th Jan. 2024
Revised	:	27th May 2024
Accepted	:	22nd Oct. 2024
Published	:	15th Nov. 2024

KEYWORDS

Magnetorheological fluid
Magnetorheological damper
Flow rate
Velocity
Valve

1. INTRODUCTION

The suspension system of conventional vehicles often employs hydraulic dampers. However, achieving optimal driving comfort and handling stability can be challenging due to fixed spring stiffness and limited dynamic range. MR dampers have advantages over conventional hydraulic dampers, such as a simple design, quick response, damping solid force, and adjustable properties [1-3]. These devices serve as outstanding semi-active damping devices with extensive applications in transportation and beyond, such as improving vehicle comfort and ride quality in automobile suspension systems [4-6]. The working mechanism of an MR damper is equivalent to that of a viscous damper (passive damper), which provides damping force via flow limitations. A conventional viscous damper uses a flow limiter valve through an orifice channel. The flow limitations of a traditional passive damper remain constant due to the fixed orifice channel of the valve. By maintaining a consistent gap size for each MR valve channel, the MR damper precisely controls the magnetic field intensity exclusively within the flow channel [7]. Furthermore, the MR damper productivity is determined by the MR valve's capability to produce enhanced flow limitation [8].

The MR damper is an advanced system that incorporates Magnetorheological (MR) fluid, allowing for the regulation of the fluid's rheological behavior using magnetic field manipulation. MR fluid consists of carbonyl iron particles (CIP) that are immersed with the fluid, and the CIPs line up with the magnetic field presented, thus changing the fluid yield stress. MR fluid is classified as a '*smart material*', demonstrating alterations in its rheological characteristics when subjected to a magnetic field. The MR fluid is produced by combining a mixture of iron particles in micron-sized and carbonyl oil. The fluid iron particles inside vary in size, ranging from 1 to 10 microns [9]. The fluid rheological characteristics are particularly impacted by magnetic fields, which increase the fluid viscosity [10-12]. The MR fluid clutch was introduced by Jacob Rainbow in 1948 and has been widely used in the commercialized industry for the past decade [12-13]. During exposure to a magnetic field, the fluid rapidly reacts within 10 milliseconds and intensifies as the iron particles organize together into a structure like a chain. This effect can be attributed to the simple (direct), fast, and robust interface between the mechanical components and the electric control [14-15]. Furthermore, MR fluid is being utilized in various automotive components, including vehicle clutches, brakes, steering systems, suspension systems, and engine mounts, demonstrating exceptional electromechanical responses within these systems [16-20]. The MR damper is a widely known device that uses an MR fluid and has been extensively studied over the last decade [21-25]. The MR damper is now available for high-end passenger automobiles, offering semi-active and active suspension systems [24].

*CORRESPONDING AUTHOR | A.Z. Zainordin, Z. Mohamed | ✉ zaifazlin@polisas.edu.my, zamrim@umpsa.edu.my

Several MR valve designs for dampers have been previously recommended. Previously, Kordonski [25] presented a stand-alone MR valve and devices with magnetorheological elements, and Gorodkin [26] extended this concept to a passive damping mechanism for MR throttle valves. Yokota [27] presented an innovative control valve for fluid control systems. This valve operates with an MR fluid with an electromagnetic coil adjacent to the flow channel. Later, Yoshida [28] further enhanced a compact three-port MR valve by adding a permanent magnet, reducing its overall size, and modifying it for a bellows-driven motion control system. Grunwald and Olabi [9] analyzed the MR valve performance by evaluating both its annular and orifice variations. Furthermore, Ai [7] and Wang [29] examined the MR valve type and studied design variations involving annular and radial flow routes. Imaduddin et al. [8] proposed incorporating several annular and radial gaps into an external MR valve compact design. The proposed approach enabled the achievement of a higher pressure drop while maintaining the outer valve diameter size. The pressure drop rating of a three-phase modular design was assessed using an independent stage MR valve modular with a meandering flow route, as proposed by Ichwan et al. [30]. In 2020, Hu et al. [31] studied the flow channels in car suspension systems. They employed a mixture of magnetic and non-magnetic components in the piston head to create three adequate damping gaps. Their proposed valve, operating at 1.5 A, achieved a damping force of 6.8 kN, demonstrating its robust vibration control mechanical attributes. Idris et al. [32] explored a novel concentric bypass MR damper design featuring a serpentine flux valve positioned within the bypass channel in alignment with the cylinder axis. This serpentine valve design offers 1.5 times better dynamic range performance than the traditional structure, implying the potential for substantial enhancements in the MR damper design.

This work aims to study the characteristics of a small core annular radial magnetorheological valve (SCARMV). The valve structure of the damper contains a compact core that combines annular and radial fluid flow routes. Some modifications to the valve geometry are done based on the results of an actual experiment and simulation software (FEMM). One of the main parameters of the MR fluid yield stress is predicted based on the applied current. Different currents and frequencies were used in the experimental testing of the MR valve dampers. The MR valve equation was calculated, and the results were compared to experimental data. The damper force effect at the high current was then investigated through an experimental evaluation of the MR valve damper's performance.

2. MR VALVE STRUCTURES

A new SCARMV design as an internal valve for dampers is introduced in this work. The design idea was based on the meandering flow type, which consists of multiple valve cores, which are simplified to a single core. The simplified small valve core, which consists of an annular and radial fluid flow gap, is tested for a single tube damper. Figure 1 illustrates the proposed MR valve designs for an internal damper consisting of an annular and radial fluid flow inside the piston. The MR damper consists of several parts: an MR valve piston, piston rod, top cover, damper housing, accumulator piston, and bottom cover, as shown in Figure 1(a). Next, the outer diameter of the MR valve piston is designed to fit a sedan car's standard shock absorber housing. The MR valve's outer diameter measures 47 mm, corresponding to the internal diameter of the PROTON Waja absorber. Most damper components were fabricated using AISI 1018 mild steel and only for a coil bobbin, and the piston connecting rod was made from Stainless Steel 316 (non-magnetic material), which was selected based on its magnetic and non-magnetic properties, cost-effectiveness, permeability, and wide availability [33]. MRF132DG was employed to energize the damper under an apparent magnetic field [34], and the MR fluid properties are listed in Table 1.

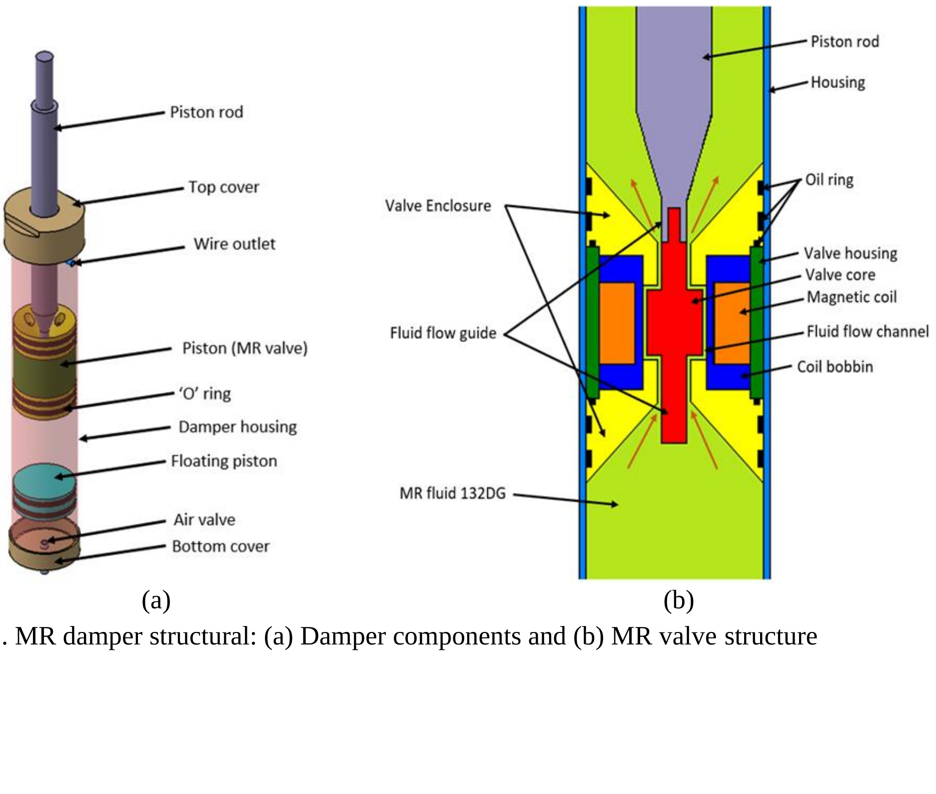

(a) (b)

Figure 1. MR damper structural: (a) Damper components and (b) MR valve structure

Table 1. MR132DG Properties [34]

Appearance	Dark Gray Liquid
Viscosity, Pa-s @ 40°C (104°F)	0.112 ± 0.02
Calculated as slope 800-1200 sec-1	
Density	2.95-3.15 (g/cm3)
	24.6-26.3 (lb/gal)
Solid content by weight	80.98%
Flash Point	>150 (°C)
	>302 (°F)
Operating Temperature	-40 to +130 (°C)
	-40 to +266 (°F)

Figure 1(b) displays the primary valve structure within the piston, while Figures 2 and 3 display the actual main components of the MR valve after fabrication. The valve comprises an upper and lower enclosure, valve core, valve housing, and coil bobbin. The valve core's height is 37 mm, its outer annular diameter is 7 mm, and its inner annular diameter is 14 mm. The outer and inner annular regions are 10 and 15 mm in length, respectively. The valve core was embedded in a spacer with a height of 1 mm to facilitate fluid flow in the radial area. Moreover, the valve core is elongated by 10 mm to promote fluid flow and acts as a guide during compression and extension movements. Then, the valve is placed in the middle of the coil bobbin and secured to the enclosure using an M4 screw with a 7-mm thread for proper fitting. The enclosure design also includes a 45° funnel to channel fluid into the valve gaps and assist with flow through the minor gaps. The valve enclosure has two 42 mm oil rings that encircle both the upper and lower sides. The purpose of these rings is to block fluid flow between the damper housing and piston, resulting in a decreased pressure drop and affecting the damping force. The coil bobbin also comes with an outer valve housing to prevent fluid from entering the coil area. Additionally, each component is fabricated using a high-precision turning machine with a fitting tolerance of approximately 6μm.

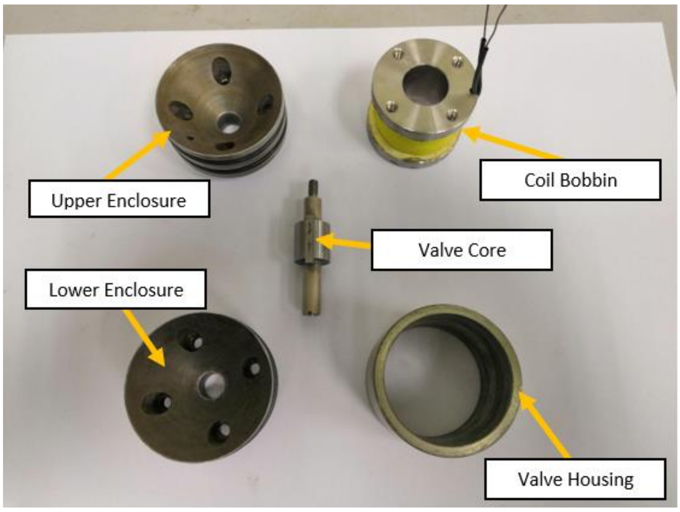

Figure 2. SCARMV main components

The single tube damper for the MR valve has a diameter of 50 mm outer and 47 mm inner diameter, matching the valve's outer diameter in Figure 3. A single-tube damper requires an accumulator to maintain pressure during valve movement. The air pressure was introduced through the air inlet valve on the bottom damper cover to pressurize the accumulator chamber. The piston rod, which is 20 mm in diameter and 186 mm in length, is connected to the piston (MR valve) using a threaded screw. This connection allows dynamic valve movement during damper testing. On the other hand, the top cover uses a dual oil seal to prevent fluid leakage during rod movement. Next, the magnetic coil wire outlet was located on the upper side of the housing, as depicted in Figure 1(a). Figure 1(b) illustrates that fluid enters the gaps stated by the red arrow during the compression stroke and flows from the lower to the upper channel gap. The green area emphasizes the MR fluid flow's effective gap.

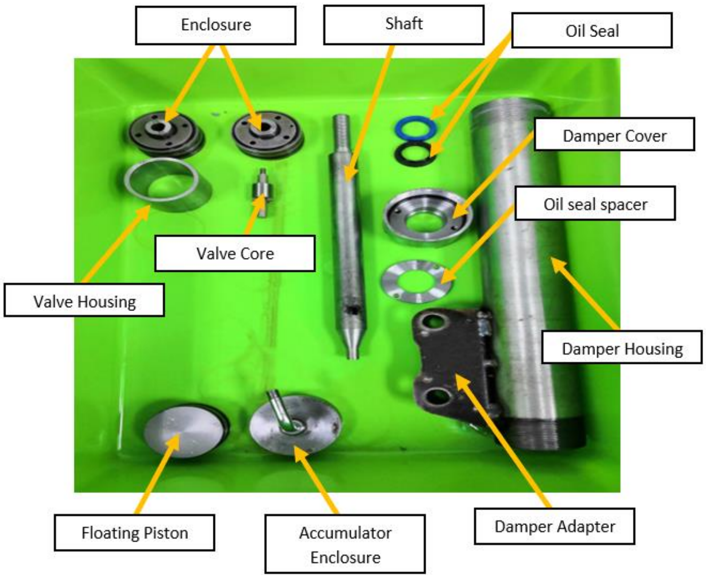

Figure 3. MR damper components

3. MAGNETIC DISTRIBUTION ANALYSIS IN MR VALVES

The magnetorheological valve magnetic modeling utilized a finite element magnetic method (FEMM) to predict the magnetic field's existence within the valve's active area. This approach is generally employed during the first stage of the design of MR devices [8], [35]. Besides, the magnetic field's appearance measurement is challenging experimental and requires simulating it using FEMM software to predict the distribution of magnetic flux. Structural and thermal responses were not considered in this model. The simplest technique to evaluate the MR impact of a fluid is by studying the magnetic circuit. To avoid any interaction between the magnetic copper wire and the steel, the coil bobbin is made of stainless steel type 314, which is a non-magnetic material. Furthermore, the piston rod is constructed using an identical coil bobbin material to effectively inhibit magnetic leakage toward the rod.

Table 2. MR damper magnetic components and properties

No.	Element	Material	Magnetic Properties
1.	Upper and lower enclosures	Steel standard ANSI 1018	Magnetic
2.	Valve core	Steel standard ANSI 1018	Magnetic
3.	Valve housing	Steel standard ANSI 1018	Magnetic
4.	Outer housing	Steel standard ANSI 1018	Magnetic
5.	Damper housing	Steel standard ANSI 1018	Magnetic
6.	Bearing	Mild Steel	Magnetic
7.	Coil wire	Copper	Magnetic
8.	Coil bobbin	Stainless Steel 316	Non-magnetic
9.	Piston rod	Stainless Steel 316	Non-magnetic
10.	Oil seal	Silicone	Non-magnetic

The simulation in this study required the assignment of several variables, as indicated in Table 2. The coil contains 300 turns and consists of a copper wire type 22 AWG with a diameter of 0.644 mm. The magnetic analysis revealed a coil resistance of 1.52 Ohms. This analysis sets a limit of 1 A for the current and 1.52 watts for the valve power consumption. The valve was constructed in the FEMM through 2D axisymmetric triangular elements, resulting in 23,717 elements and 12,053 nodes in the simulation, as illustrated in Figure 4(a). Figure 4(b) displays the density of the magnetic flux contour, where the valve's active area is surrounded by the flux lines. Consequently, the MR fluid yield stress can be altered by passing a magnetic flux through each gap. The area in which the magnetic flux lines navigate through annular and radial gaps without significant losses is called the "active" area. By adjusting the current input, the fluid rheological behavior can be manipulated. Furthermore, the MR valve flow path implies that the MR fluid must cross a junction between annular and radial channels. According to the findings of [6], one way to enhance the pressure drop and increase the damping force in an internal MR damper is to use a combination of annular and radial valve modes.

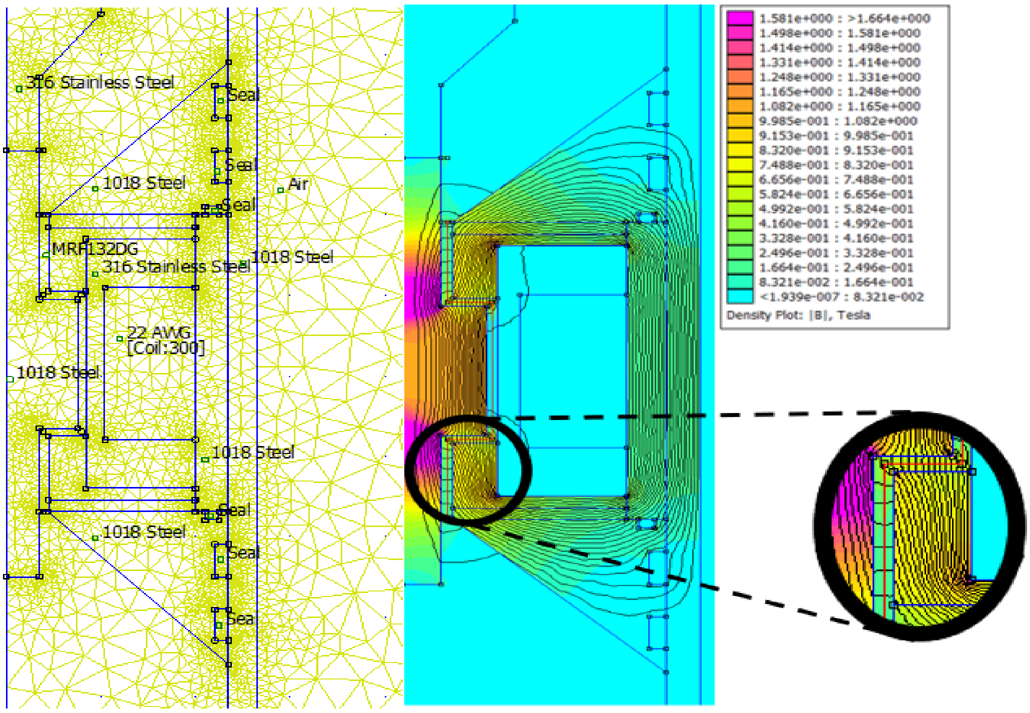

(a) (b)

Figure 4. Finite element magnetic analysis: a) 2D axisymmetry model b) 2D flux lines

Figure 5(a) indicates the magnetic simulation results, emphasizing the fluid movement channel. The magnetic flux density proportionally increases with the current when the applied current is starting 0.2 A to 1 A in steps of 0.2 A. The density variance of the magnetic flux describes the variation between the upper and lower annular gaps, the inner radial, and the inner annular gaps. In FEMM, the inner radial gap has a higher density of magnetic flux than the annular gap and inner annular gaps. The magnetic flux density at the outer annular gap is 0.29 T and 0.67 T at the inner radial gap when 1 A current was used. The inner radial gap demonstrated greater magnetic flux density at 1 A current than the outer annular gap. From Figure 5(b), the magnetic field slightly increased slowly when the current was applied, 0.8 A to 1 A, because the magnetic field started to saturate and differed with the radial gaps. Nonetheless, minimal magnetic flux densities are observed in the inner annular gaps, which can be neglected.

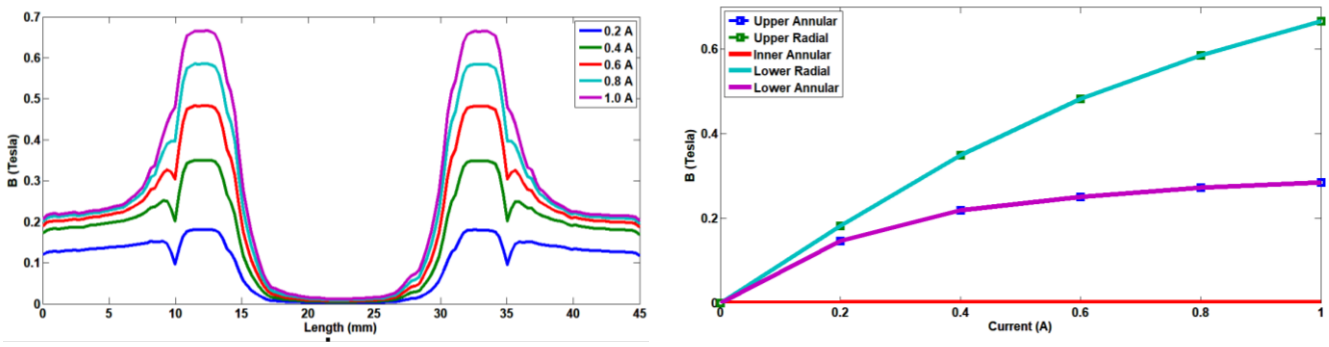

(a) (b)

Figure 5. Magnetic flux density at various currents; (a) Predicted magnetic flux density within the valve gaps and, (b) The density of magnetic flux variation in each gap

The MR fluid yield stress derived from the simulation was subsequently applied to compute the density of magnetic flux surrounded by each gap. The MR fluid yield stress is affected by the magnetic field applied to the MR valve. Modifying the apparent magnetic field can modify the yield stress of the fluid properties within the valve. Commercial MRF-132DG data was utilized in this research [34]. The magnetic flux density and yield stress relationship in an MR fluid is expressed by a third-order polynomial in Equation (1) [35]:

$$\tau_y(B) = \begin{cases} -58.92B^3 + 74.66B^2 + 35.74B - 3.387, & for\ (B) > 0 \\ 0 & for\ (B) \leq 0 \end{cases} \tag{1}$$

Magnetic flux density (B) determines MR fluid yield stress (τ_y), with three different magnetic flux densities at the annular, radial, and inner annular gaps. As a result, the calculated fluid yield stress must vary. Furthermore, the governing equation for pressure drop differs between gaps. The MR valve governing equation can be classified into three categories: outer annular, radial, and inner annular. The predicted magnetic flux density obtained from the fluid flow path is shown in Figure 6. The yield stress has no effect on the magnetic field at the inner annular gaps because the magnetic flux passing through these gaps is the lowest. The increase in current from 0.6 A to 1 A had a small magnetic flux density effect on the outer annular gaps, as shown by the smallest diameter valve core in Figure 5, as well as at the upper annular region, where some of them diverged towards the piston rod and flow guide, which had less effect on the magnetic flux distribution within these gaps. The magnetic flux density distribution at these inner circular gaps was negligible and could be ignored. At both the upper and lower annular gaps, the inner radial gaps experience magnetic fluxes as high as 0.67 T at 1 A current.

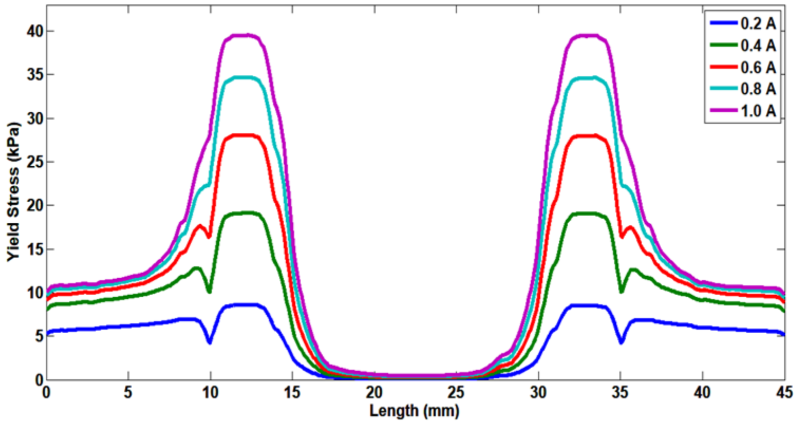

Figure 6. Prediction of fluid yield stress within the MR valve gaps

4. MR VALVE MATHEMATICAL MODEL

The fluid viscosity and the magnetic field affecting pressure drop were the two factors determining the MR damper performance. Firstly, the fluid viscosity pressure drop was determined by the fluid viscosity and flow velocity at the inlet section of the valve. Second, the magnetic field effect pressure drop can affect the fluid yield stress. The damping force in compression and extension (rebound) mode can be obtained by multiplying the active channel gap area with an attainable pressure drop. The valve pressure drop consisted of fluid viscosity and field-dependent yield stress [32]. The equations presented by Ai et al. in 2006 show the general form of obtaining MR valve pressure loss in the annular and radial gaps, as shown in Table 3 [7][29].

Table 3. Pressure drop formulas for annular and radial flow

Pressure Drop	Annular		Radial	
Viscosity, $(\boldsymbol{B}) = \boldsymbol{0}$	$\frac{6\eta QL}{\pi d^3 R}$	(2)	$\frac{6\eta QL}{\pi d^3} ln\left(\frac{R_0}{R_i}\right)$	(4)
Magnetic field, $(\boldsymbol{B}) > \boldsymbol{0}$	$\frac{c\tau(B)L}{d}$	(3)	$\frac{c\tau(B)}{d}(R_o - R_i)$	(5)

The direct pressure drop correlation between fluid viscosity (η), length of channel (L), and flow rate (Q) are explained in Equation (2). It is inversely proportional to the cube power of the valve gap (d) and channel radius (R). Contrarily, the pressure drop in Equation (3), which is dependent on the magnetic field, is directly proportional to the length of the annular channel (L), the value of yield stress ($\tau(B)$), and flow velocity profile coefficient (c) of the MR fluid, which exhibits an inverse relationship with the magnitude of the gap size (d). The coefficient (c) was calculated by assessing the ratio of the field-dependent to the viscosity-induced pressure drop using the estimated function presented by Nguyen et al. (2008) in Equation 6 [36].

$$c = 2.07 + \frac{12Q\eta}{12Q\eta + 0.8\pi R d^2 \tau(B)} \tag{6}$$

Nonetheless, Equations (2) and (3) specifically apply to MR valves with annular gaps. For MR valves featuring radial gaps, the equations describing the viscous and yield pressure drop can be derived by following the approach outlined by Wang et al. (2009) [29]. The notation “valve gap size (d)” in Equations (5) and (6) corresponds to radial gaps, while “Ro” and “Ri” represent the outer and inner radii of these gaps. Equations (7)–(10) must be included in the mathematical formula for the pressure loss in the proposed MR valve design to describe the annular and radial gaps. Nevertheless, to simplify the derivation process, the valve gaps are classified into three distinct areas: the outer annular, inner radial and inner annular gaps, as demonstrated in Figure 7. This division was necessary because each area was expected to exhibit varying magnetic flux levels. Furthermore, these three areas can be further separated into two categories: those designated as having an effective area and those defined by only the viscous resistance pressure drop. In Figure 7, the annular gaps are marked in yellow, the radial gaps in blue, and the inner annular gaps in green.

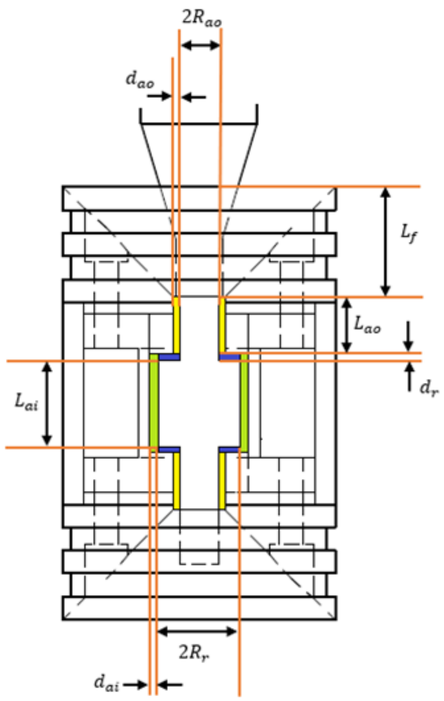

Figure 7. Dimension of MR valve

The practical areas include the outer annular and inner radial gaps, with the inner annular area primarily contributing to the viscous resistance. Equations (8)–(10) provide the formulas to compute the MR valve pressure drop at each gap, accounting for both annular and radial pressure drops. The following equations can express the MR valve pressure drop [8], [32]:

$$\Delta P_T = \Delta P_{annular_{upper}} + \Delta P_{radial_{upper}} + \Delta P_{inner_{annular}} + \Delta P_{radial_{lower}} + \Delta P_{annular_{lower}} \tag{7}$$

$$\Delta P_{outer_{annular}} = 2\left[\frac{6\eta Q L_{ao}}{\pi {d_{ao}}^3 R_{ao}} + \frac{c_{ao}\tau(B)L_{ao}}{d_{ao}}\right] \tag{8}$$

$$\Delta P_{radial} = 2\left[\frac{6\eta Q}{\pi {d_r}^3}\ln\left(\frac{R_r}{R_{ao}}\right) + \frac{c_r\tau(B)}{d_r}\ln(R_r - R_{ao})\right] \tag{9}$$

$$\Delta P_{Inner_{annular}} = \left[\frac{6\eta Q L_{ai}}{\pi {d_{ai}}^3 R_{ai}}\right] \tag{10}$$

The gap-size thickness and the magnetic field strength in both annular and radial configurations substantially influence the attainable pressure drop. Using the FEMM analysis, the MR valve model was estimated with varying magnetic field strengths, allowing for the prediction of fluid yield stress based on the simulation results. Based on the specification data for MRF-132DG, a nonlinear relationship can be observed between the magnetic field strength and fluid yield stress. The MR damper parameters are detailed in Table 4 and are incorporated as the actual simulation model parameters. The equation of flow rate is given by Equations (11)–(13), where (A) is the effective MR valve gaps and (v) is the fluid velocity that enters the gaps. The value was obtained from the experimental data.

Table 4. MR damper parameters

Parameters	Description	Units	Value
$\eta\ (MRF-132DG)$	Viscosity of the fluid	[Pa.s]	0.112
L_{ao}	Outer annular channel length	[mm]	10.0
L_{ai}	Inner annular channel length	[mm]	15.0
$d_{ao} = d_r = d_{ai}$	Annular and radial gap sizes	[mm]	1.0
R_{ao}	Outer annular radius/ inner radial radius	[mm]	3.5
$R_r = R_{ai}$	Outer radial radius /Inner annular radius	[mm]	7.0

$$Q = Av \tag{11}$$

$$Q_{in} = Q_{out} \tag{12}$$

$$v_{in}A_{in} = v_{out}A_{out} \tag{13}$$

5. EXPERIMENTAL METHOD

The characteristics of the MR valve damper were tested under various frequencies and currents using a dynamic test machine (Shimadzu EHF-L series) that is available at the Universiti Teknologi Malaysia, as shown in Figure 8. The MR damper characteristics were assessed by connecting the prototype to a testing machine. The MR valve was fixed to the damper shaft for dynamic movement, and the shaft was attached to the hydraulic cylinder actuator on the upper side of the machine. Lord Corporation's MRF132-DG was utilized as the medium to energize the damper. The damper body was then affixed to the adapter connected to the load cell at the machine's bottom. The load cell measures the damping force reaction under various inputs. The data from the measurement sensors is collected and transferred to a personal computer via a servo controller 4830 through a communication port connected to the host PC. The measurement data is recorded by the servo controller software and then transferred to the host PC for analysis. Furthermore, the single-tube damper requires an accumulator to maintain the pressure during compression and rebound movements.

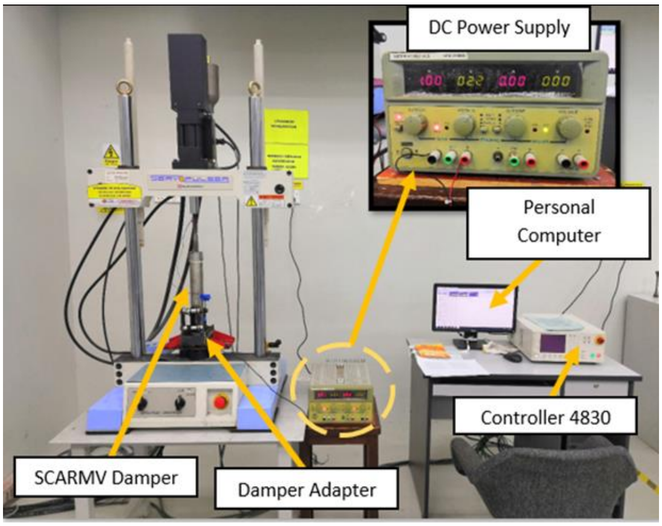

Figure 8. Shimadzu testing machine

The accumulator chamber was air-pressurized to 1 bar through the air-inlet valve. Next, to power the electromagnetic coils in the MR valve, GW-INSTEK’s regulated DC power supply was employed to energize the valve coil. The stroke length was set to 10 mm during testing, and the frequency was set to 0.5 Hz and 1.0 Hz. The current supplied to the magnetic coil was increased by 0.2 A, from 0 A to 1 A. To ensure good repeatability, the sampling rate for each data point was 1000 samples per sinusoidal cycle, with 20 cycles tested for current and stroke. There is a difference in coil resistance between the experimental and simulation results in Figure 8. The coil resistance was roughly 2.2 ohm, whereas the simulation produced a resistance of 1.52 ohm, neglecting the air gap between the coil layers. The difference was approximately 69.1% compared to the experimental measurements.

6. MR DAMPER CHARACTERISTICS

The evaluation of the SCARMV damper's performance under dynamic sinusoidal excitation is described in this section by utilizing the force-displacement curve at different currents and frequencies. The damping characteristics for a 10 mm amplitude are shown in Figures 9 and 10 for force-displacement and force-velocity, with sinusoidal excitations of 0.5 and 1 Hz. The currents were 0.2 A, 0.4 A, 0.6 A, 0.8 A, and 1 A. As the current increases, this affects the damping force. At 0 A current, the damping force without a magnetic field is 540 N (compression) and 250 N (rebound) at 0.5 Hz. The damping force increased to approximately 940 N (compression) and 600 N (rebound) when the frequency rises to 1 Hz. The proportionally damping force increases as the current increases from 0.2 A to 1.0 A. At 1 A, the maximum damping force on the compression side is 1570 N, and on the rebound side, it is 1350 N for 1 Hz frequency. When 1 A of current was applied at 0.5 Hz, the damping force difference was approximately 74.4% on the compression side and 82.8% on the rebound side, relative to the higher frequency testing. Moreover, a higher damping force at the compression side is commonly produced by the commercialized MR damper compared to the rebound side. Conversely, the compression side exhibits a slightly greater damping force than the rebound side due to the weight of the piston and piston rod. Another consideration is the variation in fluid volume between the upper and lower chambers, which affects the damping force.

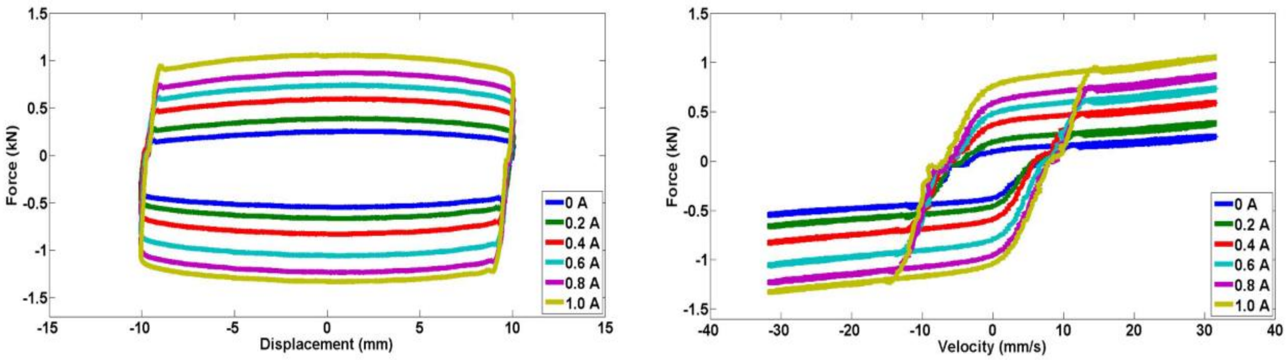

(a) (b)

Figure 9. Performance of damping force under an applied current of 10 mm displacement at 0.5 Hz frequency; (a) Force versus displacement and, (b) Force versus velocity

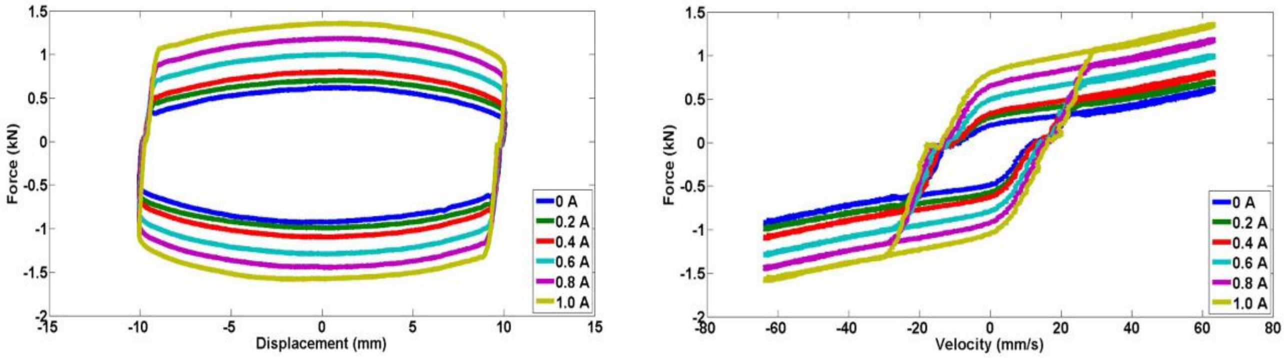

(a) (b)

Figure 10. Performance of damping force under an applied current of 10 mm displacement at 1.0 Hz frequency; (a) Force versus displacement and, (b) Force versus velocity

The damping force performance under a selected current with 0.5 Hz frequency and 10 mm amplitude is shown in Figure 11. It is observed that the damping force increases in proportion to the rises of current, following a similar trend but with different force values. Current values of 0 A, 0.4 A, and 0.8 A were selected, resulting in damping forces of 540 N, 850 N, and 1210 N on the compression side. The rebound side is 250 N, 600 N, and 900 N, indicating that the compression side produced a slightly higher damping force than the rebound side at 74.4% concerning 1 A of supply current. Moreover, as depicted in Figure 12, the damping force increases steadily when the frequency is increased to 1 Hz. At a frequency of 1 Hz, the generated damping forces are 922 N, 1100 N, and 1440 N during compression and 610 N, 830 N, and 1180 N during rebound, with applied currents of 0 A, 0.4 A, and 0.8 A, respectively. At frequencies of 0.5 and 1 Hz, the valve velocities were measured as 31.7 mm/s and 63.7 mm/s. The valve velocity, as mentioned in Equation 13, will be employed in the simulation model to calculate the fluid flow rate.

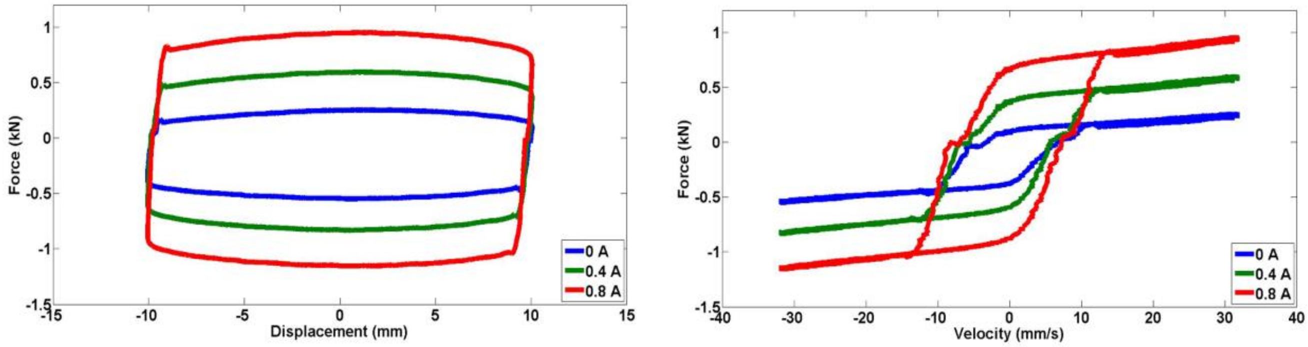

(a) (b)

Figure 11. Performance of damping force under a selected current of 10 mm displacement at 0.5 Hz frequency; (a) Force versus displacement and, (b) Force versus velocity

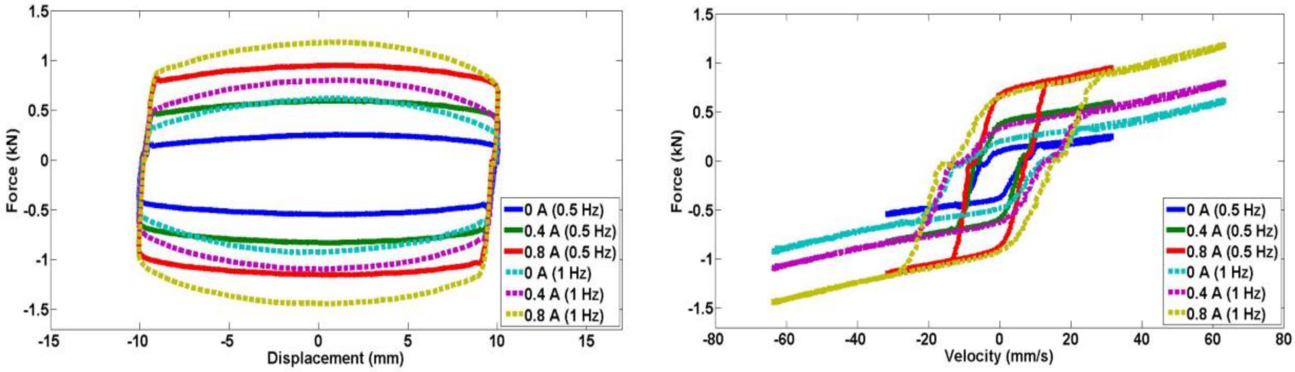

(a) (b)

Figure 12. Performance of damping force under a selected current of 10 mm displacement at 0.5 Hz and 1 Hz frequency; (a) Force versus displacement and, (b) Force versus velocity

The MR valve damper's mathematical model is validated by comparing it with experimental data. The comparison between the simulation and experiment results for the damping force for 0.5 Hz and 1.0 Hz is depicted in Figure 13 at various currents. The damping force at different currents and frequencies yields the measured data, as shown in Figure 12. Agreement between the analytical model simulation and experimental data was acceptable, closely aligning with incremental trends. When current and frequency increase, the damping force also increases. A slight discrepancy between simulation and experimental data can be observed when the current rises. The experimental damping force slightly exceeded the simulated because of the friction between the O-rings of the piston enclosure and the valve components. The simulation model neglected the sealing fiction and accumulator force impacts. Another factor that leads to a higher damping force in the compression stroke than in the rebound stroke is the difference in fluid volume between the upper and lower chambers.

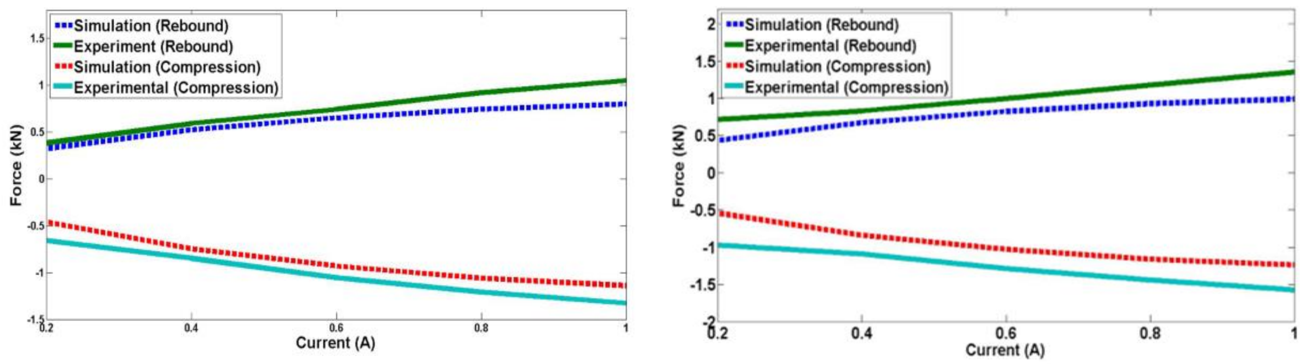

(a) (b)

Figure 13. Damping force comparison between simulation and experimental under an applied current of 10 mm displacement; (a) 0.5 Hz and, (b) 1.0 Hz

The simulation-predicted damping force was compared with the experimental results to verify the mathematical model of the proposed valve. The deviation between the simulation and experimental results can be evaluated using relative error values. The relative errors of the MR valve dampers at an amplitude of 10 mm are shown in Tables 5 and 6 for frequencies of 0.5 Hz and 1 Hz. The relative error between the experiment and simulation was calculated using the following formula [30]:

$$\epsilon = \frac{F_{experiment} - F_{Simulation}}{F_{experiment}} \tag{14}$$

The observed discrepancy can be used to explain several possibilities. The model does not fully consider parameters such as magnetic properties, fluid and flow characteristics, and geometrical valve size. The fluid viscosity and magnetic effects generally cause variations in the error valve. The experimental data show a slightly higher disagreement than the simulation, which does not account for certain parameters. At 0 A of current, the difference between the simulation and experimental was more significant than the applied current. This occurs because the damping values vary between the off and on states. The relative error decreased when the current was increased with the excitation frequency. The relative error decreased as the current increased but increased with higher frequencies.

Table 5. Relative error between simulation and experimental results for 0.5 Hz at 10 mm amplitude

Current (A)	Rebound			Compression		
	Experiment (kN)	Simulation (kN)	Error (%)	Experiment (kN)	Simulation (kN)	Error (%)
0	0.25	0.09	64	0.54	0.27	50
0.2	0.38	0.32	16	0.66	0.46	31
0.4	0.59	0.52	11	0.85	0.75	12
0.6	0.74	0.65	12	1.06	0.93	12
0.8	0.92	0.74	19	1.21	1.06	12
1.0	1.05	0.80	24	1.33	1.14	14

Table 6. Relative error between simulation and experimental results for 1.0 Hz at 10 mm amplitude

Current (A)	Rebound			Compression		
	Experiment (kN)	Simulation (kN)	Error (%)	Experiment (kN)	Simulation (kN)	Error (%)
0	0.61	0.18	70	0.92	0.34	63
0.2	0.71	0.43	39	0.97	0.54	45
0.4	0.83	0.67	19	1.09	0.84	23
0.6	0.99	0.82	17	1.29	1.03	20
0.8	1.18	0.93	21	1.44	1.16	20
1.0	1.35	0.99	27	1.57	1.24	21

Magnetic leakage is another factor that differentiates simulations from experimentation. Magnetic analysis revealed that the magnetic flux lines leak at the inlets and outlets, as demonstrated in the magnetic simulation results. Energization of the MR fluid can occur before it enters the valve gap. The fluid flow will be interrupted as the magnetic field begins to energize. There is a higher possibility of particle clotting at each 90^0 junction when a current of 1 A is present. Furthermore, the equation does not account for the presence of a 45^0 geometrical funnel, which leads to redundancy in the force valve simulation. The funnel angle's shear effect significantly affects the fluid flow velocity before entering the valve gaps. Hence, the simulation only considered the valve core and did not consider the accumulator effects and frictional forces between the oil seal and the inner tube surface of the damper.

7. CONCLUSION

The design, fabrication, and testing of the new SCARMV has been presented. The model was developed by studying the parameters of annular and radial gaps from mathematical equations to calculate the damping force. The parameters include the design configuration, damper volume size, MR fluid selection, and coil turn number. The damper model was designed and fabricated based on magnetic analysis parameters. This SCARMV damper exhibits superior damping response at low and high frequencies for supplied current excitation. The simulation model did not account for the importance of the accumulator force, which significantly affected the damping force trend in the higher active states of the current. The output of the results distinguishes between uncontrollable and controllable damping forces with increasing current and frequency excitation. Therefore, based on the experimental results, it was concluded that the usability of a compact core MR valve is reliable. However, more in-depth studies are required before these dampers can be applied to vehicle suspension systems.

ACKNOWLEDGEMENT

This project is being carried out with funding from the Universiti Malaysia Pahang Al-Sultan Abdullah short-term grant (RDU170382). The authors are grateful to the Ministry of Higher Education and all the participants in the project.

CONFLICT OF INTEREST

The authors declare that they do not have any conflict of interest.

AUTHORS CONTRIBUTION

Ahmad Zaifazlin Zainordin: Design concept, data collection, and interpretation of results;
Zamri Mohamed: Analysis and draft manuscript preparation;
All authors reviewed the results and approved the final version of the manuscript.

REFERENCES

[1] Y. Shiao, W.H. Kuo, Q.A. Nguyen, and C.W. Lai, "Development of a variable-damping magnetorheological damper with multiple poles," *Journal of Vibroengineering*, vol. 17, no. 3, pp. 1071–1078, 2015.

[2] X.-X. Bai, W. Hu, and N.M. Wereley, "Magnetorheological damper utilizing an inner bypass for ground vehicle suspensions," *IEEE Transactions on Magnetics*, vol. 49, no. 7, pp. 3422–3425, 2013.

[3] B. Lei, J. Li, W. Zhou, M. Shou, F. Zhao, and C. Liao, "Dual-stage theoretical model of magnetorheological dampers and experimental verification," *Smart Materials and Structures*, vol. 33, no. 4, p. 045027, 2024.

[4] S. Sun, X. Tang, J. Yang, D. Ning, H. Du, S. Zhang et al., "A new generation of magnetorheological vehicle suspension system with tunable stiffness and damping characteristics," *IEEE Transactions on Industrial Informatics*, vol. 15, no. 8, pp. 4696–4708, 2019.

[5] T. Xu, H. Wang, Y. Li, D. Leng, and H. Xu, "Full vehicle experimental testing of semi-active suspension equipped with magnetorheological dampers," in *2023 IEEE/ASME International Conference on Advanced Intelligent Mechatronics (AIM)*, pp. 495–500, 2023.

[6] G. Hu, Q. Liu, R. Ding, and G. Li, "Vibration control of semi-active suspension system with magnetorheological damper based on hyperbolic tangent model," *Advances in Mechanical Engineering*, vol. 9, no. 5, 2017.

[7] H.X. Ai, D.H. Wang, and W.H. Liao, "Design and modeling of a magnetorheological valve with both annular and radial flow paths," *Journal of Intelligent Material Systems and Structures*, vol. 17, no. 4, pp. 327–334, 2006.

[8] F. Imaduddin, S.A. Mazlan, H. Zamzuri, and I.I.M. Yazid, "Design and performance analysis of a compact magnetorheological valve with multiple annular and radial gaps," *Journal of Intelligent Material Systems and Structures*, vol. 26, no. 9, pp. 1038–1049, 2013.

[9] A. Grunwald and A.G. Olabi, "Design of magnetorheological (MR) valve," *Sensors and Actuators A: Physical*, vol. 148, no. 1, pp. 211–223, 2008.

[10] G. Liu, F. Gao, D. Wang, and W.-H. Liao, "Medical applications of magnetorheological fluid: A systematic review," *Smart Materials and Structures*, vol. 31, no. 4, p. 043002, 2022.

[11] T.R.G. Chary, M. Allaparthi, S. Dusa, P. Suryapet, and D. Tarun, "Properties, applications, defects, and failures of magnetorheological fluids," in *Intelligent Manufacturing and Energy Sustainability*, Singapore: Springer Nature Singapore, pp. 517–528, 2024.

[12] H. Eshgarf, A. Ahmadi Nadooshan, and A. Raisi, "An overview on properties and applications of magnetorheological fluids: Dampers, batteries, valves and brakes," *Journal of Energy Storage*, vol. 50, p. 104648, 2022.

[13] J. Rabinow, "The magnetic fluid clutch," *Electrical Engineering*, vol. 67, no. 12, p. 1167, 1948.

[14] X. Tang, X. Zhang, R. Tao, and Y. Rong, "Structure-enhanced yield stress of magnetorheological fluids," *Journal of Applied Physics*, vol. 87, no. 5, pp. 2634–2638, 2000.

[15] S. Pisetskiy and M.R. Kermani, "A concept of a miniaturized MR clutch utilizing mr fluid in squeeze mode," in *2020 IEEE/RSJ International Conference on Intelligent Robots and Systems (IROS)*, pp. 6347–6352, 2020.

[16] D. Kumar, G.A. Harmain, G. Gaurav, K.P. Lijesh, B. Kuriachen, H. Hirani et al., "A novel seal design to enhance MR brake performance," *Transactions of the Indian Institute of Metals*, vol. 76, no. 9, pp. 2335–2342, 2023.

[17] S. Khuntia, R. Yadav, R.C. Singh, and V. Rastogi, "Design, development and analysis of a magnetorheological damper," *IOP Conference Series: Materials Science and Engineering*, vol. 804, no. 1, p. 012009, 2020.

[18] S. Chen, R. Li, P. Du, H. Zheng, and D. Li, "Parametric modeling of a magnetorheological engine mount based on a modified polynomial bingham model," *Frontiers in Materials*, vol. 6, 2019.

[19] A.Z. Zainordin, Z. Mohamed, and F. Ahmad, "Magnetorheological fluid: Testing on automotive braking system," *International Journal of Automotive and Mechanical Engineering*, vol. 18, no. 1, pp. 8577–8584, 2021.

[20] P. Raja, X. Wang, and F. Gordaninejad, "A high-force controllable MR fluid damper–liquid spring suspension system," *Smart Materials and Structures*, vol. 23, no. 1, p. 015021, 2014.

[21] Y.K. Lau and W.H. Liao, "Design and analysis of magnetorheological dampers for train suspension," *Proceedings of the Institution of Mechanical Engineers, Part F: Journal of Rail and Rapid Transit*, vol. 219, no. 4, pp. 261–276, 2005.

[22] Y.-J. Park, B.-H. Kang, and S.-B. Choi, "A new rotary magnetorheological damper for a semi-active suspension system of low-floor vehicles," *Actuators*, vol. 13, no. 4, p. 155, 2024.

[23] X. Ye, J. Dong, B. Wu, O. Qing, J. Wang, and G. Zhang, "Design and modeling of a double rod magnetorheological grease damper," *Journal of Mechanical Science and Technology*, vol. 38, no. 8, pp. 4065–4075, 2024.

[24] X. Zhu, X. Jing, and L. Cheng, "Magnetorheological fluid dampers: A review on structure design and analysis," *Journal of Intelligent Material Systems and Structures*, vol. 23, no. 8, pp. 839–873, 2012.

[25] W. Kordonski, S. Gorodkin, and A. Kolomentsev, "Magnetorheological valve and devices incorporating magnetorheological elements," Patent No. 5353839, 1994.

[26] S. Gorodkin, A. Lukianovich, and W. Kordonski, "Magnetorheological throttle valve in passive damping systems," *Journal of Intelligent Material Systems and Structures*, vol. 9, no. 8, pp. 637–641, 1998.

[27] S. Yokota, K. Yoshida, and Y. Kondoh, "A pressure control valve using MR fluid," in *Proceedings of the JFPS International Symposium on Fluid Power*, Tokyo, pp. 377–380, 1999.

[28] K. Yoshida, H. Takahashi, S. Yokota, M. Kawachi, and K. Edamura, “A bellows-driven motion control system using a magnetorheological fluid,” *Proceedings of the JFPS International Symposium on Fluid Power*, vol. 2002, no. 5–2, pp. 403–408, 2002.

[29] D.H. Wang, H.X. Ai, and W.H. Liao, “A magnetorheological valve with both annular and radial fluid flow resistance gaps,” *Smart Materials and Structures*, vol. 18, no. 11, p. 115001, 2009.

[30] B. Ichwan, S.A. Mazlan, F. Imaduddin, Ubaidillah, T. Koga, and M.H. Idris, “Development of a modular MR valve using meandering flow path structure,” *Smart Materials and Structures*, vol. 25, no. 3, p. 037001, 2016.

[31] G. Hu, H. Liu, J. Duan, and L. Yu, “Damping performance analysis of magnetorheological damper with serial-type flow channels,” *Advances in Mechanical Engineering*, vol. 11, no. 1, p. 1687814018816842, 2019.

[32] M.H. Idris, F. Imaduddin, Ubaidillah, S.A. Mazlan, and S.-B. Choi, “A concentric design of a bypass magnetorheological fluid damper with a serpentine flux valve,” *Actuators*, vol. 9, no. 1, p. 16, 2020.

[33] S. Sgobba, “Physics and measurements of magnetic materials,” in *CERN Accelerator School: Course on Magnets*, p. 25, 2011.

[34] Lord Corp, “MRF-132DG Magnetorheological Fluid,” *Lord Technical Data*, vol. 54, no. 2, p. 11, 2011.

[35] B. Ichwan, S.A. Mazlan, F. Imaduddin, H. Zamzuri, and M.A.A. Rahman, “Design and performance analysis of magnetorheological valve module with annular-radial concept,” *ARPN Journal of Engineering and Applied Sciences*, vol. 10, no. 17, pp. 7743–7748, 2015.

[36] Q.-H. Nguyen, S.-B. Choi, and N.M. Wereley, “Optimal design of magnetorheological valves via a finite element method considering control energy and a time constant,” *Smart Materials and Structures*, vol. 17, no. 2, p. 025024, 2008.